

The intermediate-age open cluster NGC 2158[★]

Giovanni Carraro¹, Léo Girardi^{1,2} and Paola Marigo^{1†}

¹ *Dipartimento di Astronomia, Università di Padova, Vicolo dell'Osservatorio 2, I-35122 Padova, Italy*

² *Osservatorio Astronomico di Trieste, Via G.B. Tiepolo 11, I-34131 Trieste, Italy*

Submitted: October 2001

ABSTRACT

We report on *UBVRI* CCD photometry of two overlapping fields in the region of the intermediate-age open cluster NGC 2158 down to $V = 21$. By analyzing Colour-Colour (CC) and Colour-Magnitude Diagrams (CMD) we infer a reddening $E_{B-V} = 0.55 \pm 0.10$, a distance of 3600 ± 400 pc, and an age of about 2 Gyr. Synthetic CMDs performed with these parameters (but fixing $E_{B-V} = 0.60$ and $[\text{Fe}/\text{H}] = -0.60$), and including binaries, field contamination, and photometric errors, allow a good description of the observed CMD. The elongated shape of the clump of red giants in the CMD is interpreted as resulting from a differential reddening of about $\Delta E_{B-V} = 0.06$ across the cluster, in the direction perpendicular to the Galactic plane. NGC 2158 turns out to be an intermediate-age open cluster with an anomalously low metal content. The combination of these parameters together with the analysis of the cluster orbit, suggests that the cluster belongs to the old thin disk population.

Key words: Open clusters and associations: general – open clusters and associations: individual: NGC 2158 - Hertzsprung-Russell (HR) diagram

1 INTRODUCTION

NGC 2158 (OCL 468, Lund 206, Melotte 40) is a rich northern open cluster of intermediate age, located low in the galactic plane toward the anti-center direction ($\alpha = 06^{\text{h}} 07^{\text{m}} .5$, $\delta = +24^{\circ} 06'$, $\ell = 186^{\circ} .64$, $b = +1^{\circ} .80$, J2000.), close to M 35. It is classified as a II3r open cluster by Trumpler (1930), and has a diameter of about 5', according to Lyngå (1987). It is quite an interesting object due to its shape, for which in the past it was considered a possible globular cluster, also presenting an unusual combination of age and metallicity. In fact it is an intermediate-age open cluster, but rather metal poor. It is a crucial object in determining the Galactic disk abundance gradient and the abundance spread at time and place in the disk.

The cluster is rather populous, and therefore it is an ideal candidate to be compared with theoretical models of intermediate-low mass stars (Carraro & Chiosi 1994a, Carraro et al. 1999). Since in the past no detailed studies have been pursued with this aim, we decided to undertake a multicolor CCD study of the cluster, which is presented in

the present paper. Moreover this paper is the third of a series dedicated at improving the photometry of northern intermediate-age open clusters at Asiago Observatory. We already reported elsewhere on NGC 1245 (Carraro & Patat 1994) and on NGC 7762 (Patat & Carraro 1995).

The plan of the paper is as follows. In Sect. 2 we summarize the previous studies on NGC 2158, while Sect. 3 is dedicated to present the observation and reduction strategies. The analysis of the CMD is performed in Sect. 4, whereas Sect. 5 deals with the determination of cluster reddening, distance and age. Sect. 6 illustrates NGC 2158 kinematics. Finally, Sect. 7 summarizes our findings.

2 PREVIOUS INVESTIGATIONS

NGC 2158 has been studied several times in the past. The first investigation was carried out by Arp & Cuffey (1962), who obtained photographic *BV* photometry for about 900 stars down to $V = 18.5$. Photographic photometry was also obtained by Karchenko et al (1997) for more than 2000 stars down to the same limiting magnitude together with proper motions.

CCD photometry in *BV* passbands was provided by Christian et al. (1985) and Piersimoni et al. (1993). Both these studies reach deeper magnitude limits. Anyhow, the former study basically provides only a selection of MS un-

[★] Based on observations carried out at Mt Ekar, Asiago, Italy. All the photometry is available at WEBDA database: <http://obswww.unige.ch/webda/navigation.html>

[†] email: giovanni.carraro@unipd.it (GC); lgirardi@pd.astro.it (LG); marigo@pd.astro.it (PM)

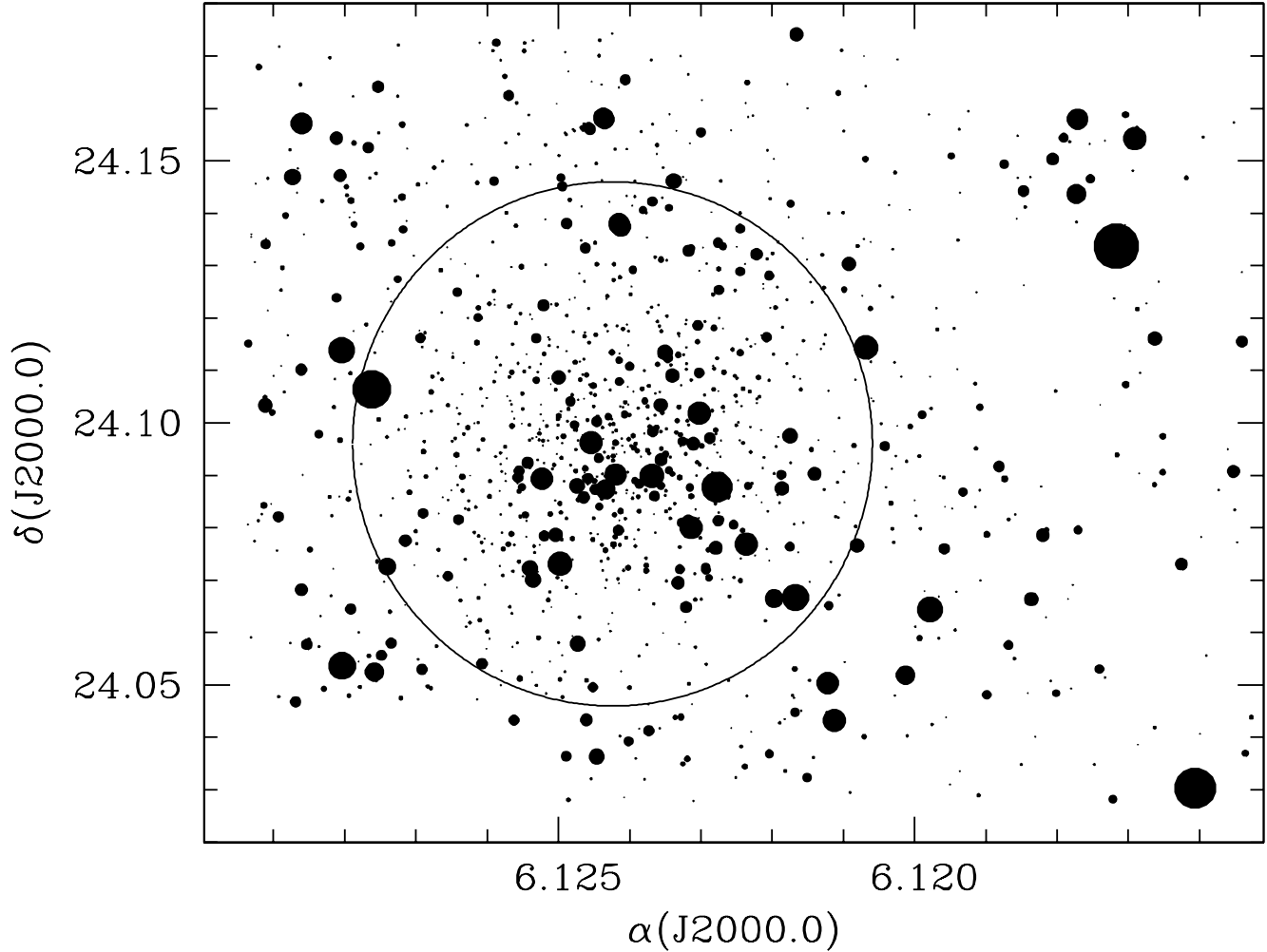


Figure 1. A V map of the observed field from the photometry of one of the deep V frames; North is up and East is to the left; the field is 9×11 arcmin². The circle confines the stars within $3'$ from the cluster center. The size of each star is inversely proportional to its magnitude.

evolved stars, whereas the latter one presents a nice CMD, but the analysis of the data appears very preliminary.

There is some disagreement in the literature about the value of NGC 2158 fundamental parameters, specially with respect to the cluster age. Estimates of cluster metallicities have been obtained by several authors, and, although different, they all point to a sub-solar metal content ($[\text{Fe}/\text{H}] = -0.60$, Geisler 1987, Lyngå 1987). Finally, the kinematics of NGC 2158 has been studied by measuring spectra of giant stars (Scott et al. 1995; Minniti 1995) to provide radial velocities. It turns out that the mean cluster radial velocity is in the range $15 - 30$ km/s (Scott et al. 1995).

3 OBSERVATIONS AND DATA REDUCTION

Observations were carried out with the AFOSC camera at the 1.82 m telescope of Cima Ekar, in the nights of January 6 and 7, 2000. AFOSC samples a $8'.14 \times 8'.14$ field in a $1K \times 1K$ thinned CCD. The typical seeing was between 1.0 and 1.5 arcsec.

For NGC 2158, typical exposure times were of 240 s

Table 1. Journal of observations of NGC 2158 (January 6-7, 2000).

Field	Filter	Time integration (sec)	Seeing ($''$)
#1	U	240	1.2
	B	300	1.3
	V	120	1.3
	R	60	1.5
	I	120	1.3
#2	U	240	1.2
	B	300	1.1
	V	120	1.3
	R	60	1.5
	I	120	1.3

in U , 300 s in B , and 60–120 s in VRI . Several images were taken, either centered on the cluster core, or shifted by about $4'$ in order to better sample the neighboring field

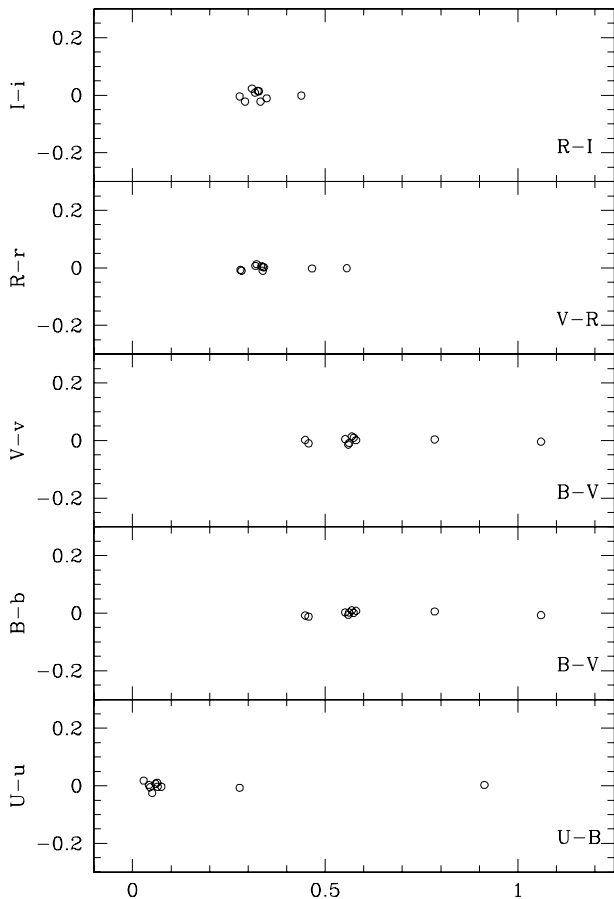


Figure 2. Differences between standard magnitudes and those obtained from our Eq. 1, for our standard stars and as a function of colour.

(see Fig. 1). However, only the images with the best seeing were used. We also observed a set of standard stars in M 67 (Schild 1983; and Porter, unpublished).

The data has been reduced by using the IRAF[‡] packages CCDRED, DAOPHOT, and PHOTCAL. The calibration equations obtained (see Fig. 2) are:

$$\begin{aligned}
 u &= U + 4.080 \pm 0.005 + (0.010 \pm 0.015)(U-B) + 0.55 X \\
 b &= B + 1.645 \pm 0.010 + (0.039 \pm 0.015)(B-V) + 0.30 X \\
 v &= V + 1.067 \pm 0.011 - (0.056 \pm 0.018)(B-V) + 0.18 X \\
 r &= R + 1.109 \pm 0.012 - (0.075 \pm 0.032)(V-R) + 0.13 X \\
 i &= I + 1.989 \pm 0.048 + (0.118 \pm 0.145)(R-I) + 0.08 X
 \end{aligned}
 \tag{1}$$

where $UBVRI$ are standard magnitudes, $ubvri$ are the instrumental ones, and X is the airmass. For the extinction coefficients, we assumed the typical values for the Asiago Observatory. Figure 2 shows the residuals of the above cali-

[‡] IRAF is distributed by the National Optical Astronomy Observatories, which are operated by the Association of Universities for Research in Astronomy, Inc., under cooperative agreement with the National Science Foundation.

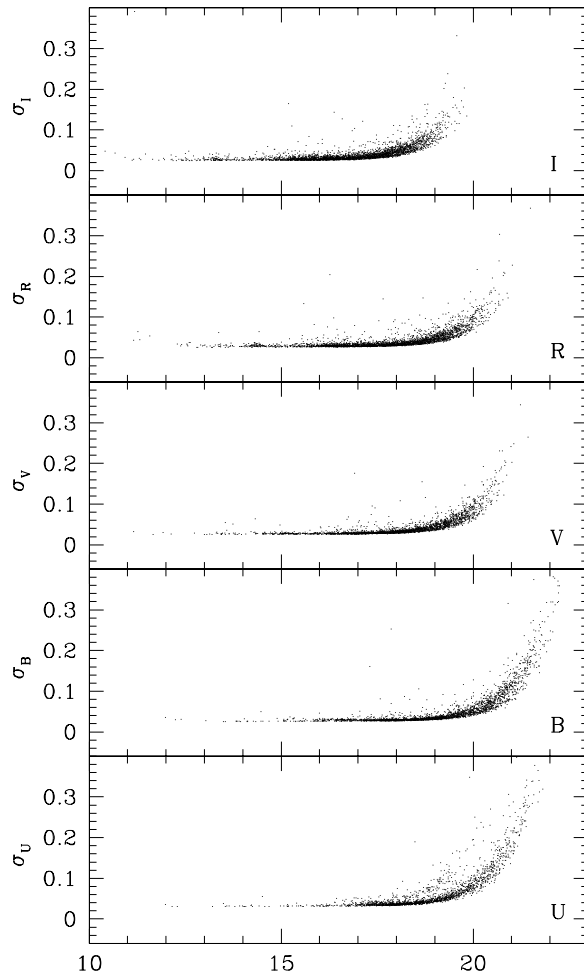


Figure 3. Photometric errors as a function of magnitude, for our NGC 2158 observations.

bration equations as a function of colour for all our standard stars.

Finally, Fig. 3 presents the run of photometric errors as a function of magnitude. These errors take into account fitting errors from DAOPHOT and calibration errors, and have been computed following Patat & Carraro (2001). It can be noticed that stars brighter than about 20 in V , R , and I , 21 in B , and U , have photometric errors lower than 0.1 mag. The final photometric data is available in electronic form at the WEBDA[§] site.

4 THE COLOUR-MAGNITUDE DIAGRAMS

A comparison of our photometry with past analyses is shown in Fig. 4, from which it is evident that the present study supersedes the previous ones. In fact, we reach $V = 21$, and are able to cover all the relevant regions of the CMD. Instead, Arp & Cuffey (1958) photometry extends only for a couple of magnitudes below the turn-off point (TO), whereas

[§] <http://obswww.unige.ch/webda/navigation.html>

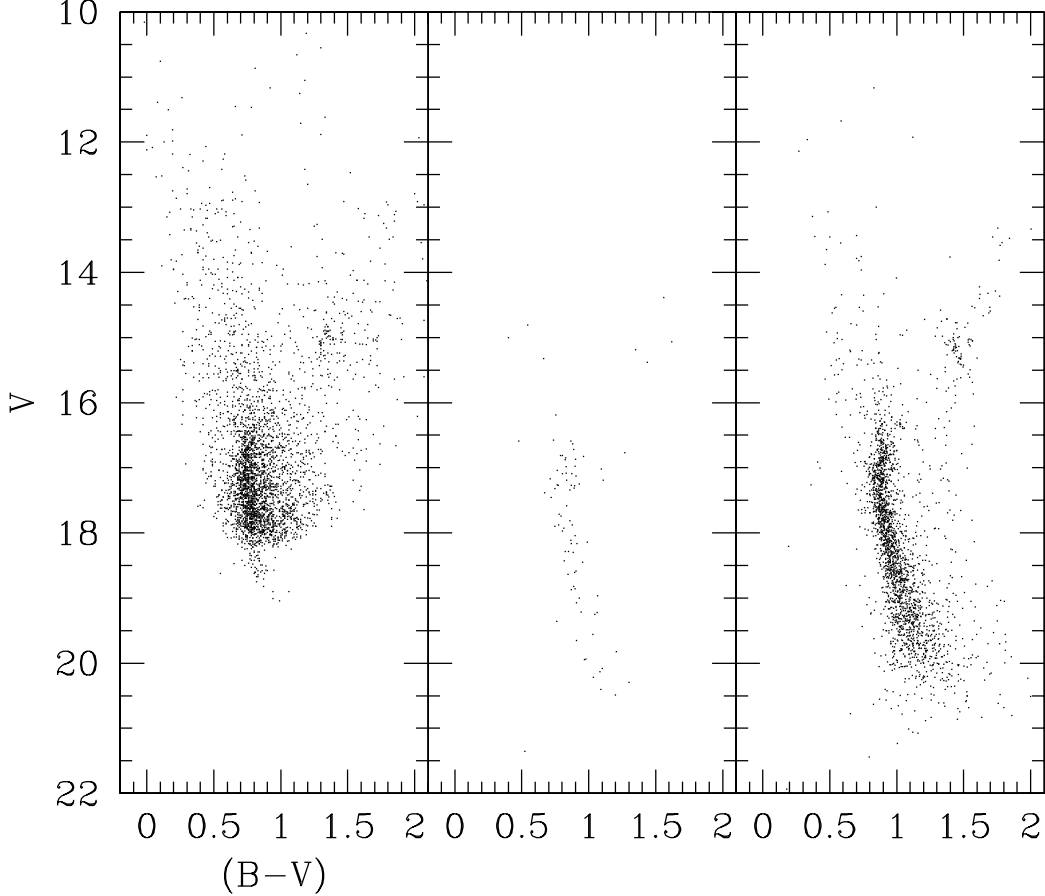


Figure 4. *BV* CMDs of NGC 2158. The left panel presents the Arp & Cuffey (1962) photometry, the central panel the Christian et al. (1985) photometry, whereas the right panel shows our photometry.

the photometry of Christian et al. (1985) does not cover the evolved region of the CMD.

To better identify the TO location and the Red Giant (RG) clump, in Fig. 5 we plot the CMDs obtained by considering stars located in different cluster regions. In details, left panel presents the CMD obtained by including all the measured stars, central panel considers the stars within a circle of radius $3'$, whereas the right panel presents only the stars located inside a circle of radius $1.5'$. The radius adopted in the central panel is compatible with the available estimate of the cluster diameter, which is about $5'$, so that we are likely considering most of the cluster members. By inspecting this CMD, we find that the TO is located at $V \approx 16.0$, $(B - V) \approx 1.0$, whereas a prominent clump of He burning stars is visible at $V \approx 15.0$, $(B - V) \approx 1.5$. The diagonal structure of this latter is probably due to differential reddening effects, which we are going to discuss in Sect. 5.3. The MS extends for 5 magnitudes, getting wider at increasing magnitudes: this is compatible with the trend of photometric errors (see Fig. 3) and the probable presence of a significant population of binary stars. The global CMD morphology resembles that of NGC 7789 (Vallenari et al. 2000) and NGC 2141 (Carraro et al. 2001), two well studied rich intermediate-age open clusters.

5 CLUSTER FUNDAMENTAL PARAMETERS

There fundamental parameters of NGC 2158 are still controversial in the literature (see Table 2). The cluster age estimates range from 0.8 to 3.0 Gyr, the distance from 3500 to 4700 pc and the reddening E_{B-V} from 0.35 to 0.55. In the next sections we are going to derive update estimates for NGC 2158 basic parameters.

5.1 Reddening

In order to obtain an estimate of the cluster mean reddening, we analyse the distribution of the stars with $V < 17$ in the $(B - I)$ vs. $(B - V)$ plane, which is shown in Fig. 6.

The linear fit to the main sequence in the $(B - I)$ vs. $(B - V)$ plane,

$$(B - I) = Q + 2.25 \times (B - V) \quad (2)$$

can be expressed in terms of E_{B-V} , for the $R_V = 3.1$ extinction law, as

$$E_{B-V} = \frac{Q - 0.014}{0.159}, \quad (3)$$

following the method proposed by Munari & Carraro (1996a,b). This method provides a rough estimate of the mean reddening and, as amply discussed in Munari & Car-

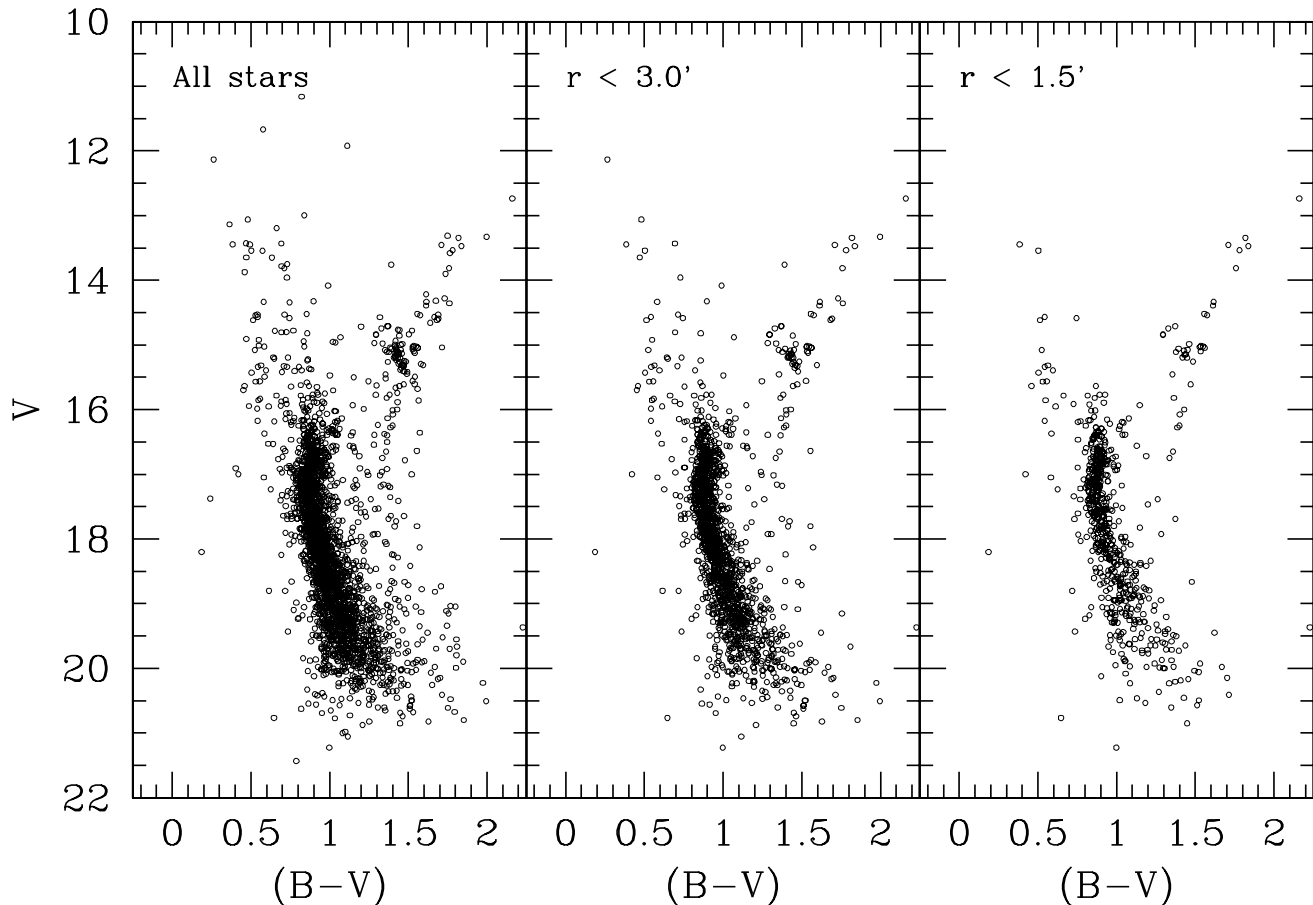


Figure 5. BV CMDs of NGC 2158. The left panel presents the CMD obtained by including all the measured stars, the central panel considers the stars within a radius of $3'$, whereas the right panel shows only the stars located inside a radius of $1.5'$.

Table 2. NGC 2158 fundamental parameters taken from the literature.

	Arp & Cuffey	Christian et al.	Kharcenko et al.	Piersimoni et al.
$E(B-V)$	0.43	0.55	0.35	0.55
$(m-M)$	14.74	14.40	13.90	15.10
distance (pc)	4700	3500	3700	4700
Age (Gyr)	0.8	1.5	3.0	1.2

raro (1996a), can be used only for certain colour ranges. In particular Eq. (3) holds over the range $-0.23 \leq (B-V)_0 \leq +1.30$. MS stars have been selected by considering all the stars within $3'$ from the cluster center and having $17 \leq V \leq 21$ and $0.75 \leq (B-V) \leq 1.25$. A least-squares fit through all these stars gives $Q = 0.097$, which, inserted in Eq. (3), provides $E_{B-V} = 0.56 \pm 0.17$. The uncertainty is rather large, and is due to the scatter of the stars in this plane, which indicates the presence of stars with different reddening, presumably a mixture of stars belonging to the cluster and to the field.

Another indication of the cluster mean reddening can be derived from the Colour-Colour diagram ($U-B$) vs. $(B-V)$, shown in Fig. 7. Here we consider again all the stars located within $3'$ from the cluster center having $17 \leq V \leq 21$ and $0.75 \leq (B-V) \leq 1.25$, to alleviate the contamination ef-

fect. The solid line is an empirical Zero-Age Main Sequence (ZAMS) taken from Schmidt-Kaler (1982), whereas the dashed line is the same ZAMS, but shifted by $E_{B-V} = 0.55$. The ratio $E_{U-B}/E_{B-V} = 0.72$ has been adopted. This shift, together with the dispersion of the data around the shifted ZAMS, provides the reddening value of $E_{B-V} = 0.55 \pm 0.10$.

5.2 Distance and age

As already mentioned, there is still a considerable dispersion in the literature among different estimates of NGC 2158 distance and age. We have derived new estimates for these parameters as follows.

First, from the Girardi et al. (2000a) database we generate theoretical isochrones of metallicity $Z = 0.0048$, that corresponds to the observed value of $[\text{Fe}/\text{H}] = -0.60$. Fig-

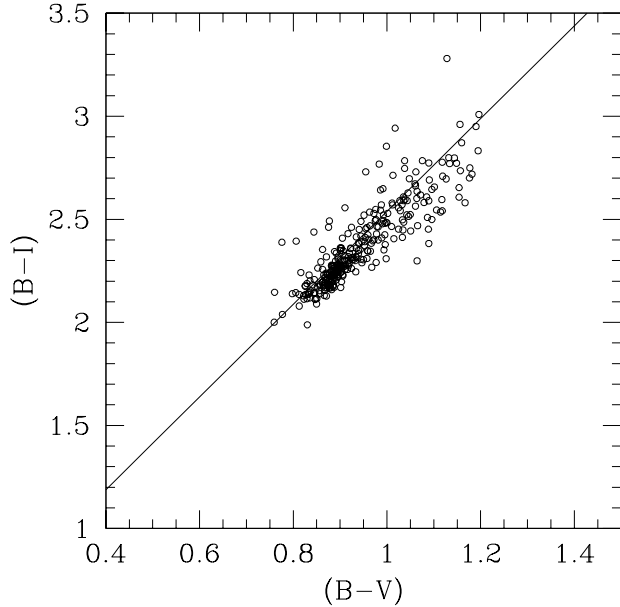


Figure 6. NGC 2158 MS stars within $3'$ in the $(B-V)$ vs. $(B-I)$ plane.

Figure 8 shows the isochrones with ages between 1.58 to 2.51 Gyr, which defines the age interval compatible with the observed magnitude difference between the red clump and the turn-off region. The isochrones were shifted in apparent magnitude and colour, until the locus of core-helium burning stars coincided with the observed mean position of the clump. The results, shown in Fig. 8, imply a true distance modulus of $(m-M)_0 = 12.8$ mag (3630 pc), and a colour excess of $E_{B-V} = 0.60$ for NGC 2158. This value is compatible with the one obtained in the previous Sect. 5.1.

It should be remarked that these are just first estimates of the cluster parameters, that we will now try to test further by means of synthetic CMDs. Figure 9 shows the sequence of steps required to simulate a CMD aimed to reproduce the NGC 2158 data. These steps are:

- The 2-Gyr old isochrone of $Z = 0.0048$ is used to simulate a cluster with 100 red clump stars. Assuming a Kroupa (2001) IMF, in order to reach this number we need an initial cluster mass of about $1.5 \times 10^4 M_\odot$, which is assumed herein-after. We have simulated detached binaries, assuming that 30 percent of the observed objects are binaries with a mass ratio located between 0.7 and 1.0. This prescription is in agreement with several estimates for galactic open clusters (Carraro & Chiosi 1998) and with the observational data for NGC 1818 and NGC 1866 in the LMC (Elson et al. 1998; Barmina et al. 2001). The result of such simulation is shown in Fig. 9(a). In this panel we can see that most of the stars – the single ones – distribute along the very thin sequence defined by the theoretical isochrone. Binaries appear as both (i) a sequence of objects roughly parallel to the main sequence of single stars, and (ii) some more scattered objects in the evolved part of the CMD.

- In order to estimate the location of foreground and background stars, we use a simple Galaxy model code (Girardi et al., in preparation). It includes the several Galac-

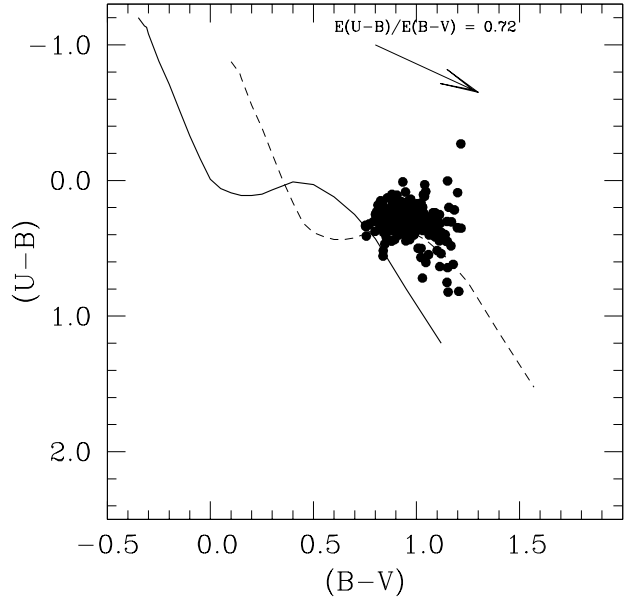


Figure 7. NGC 2158 stars within $3'$ in the colour-colour diagram. The solid line is an empirical ZAMS taken from Schmidt-Kaler (1982), whereas the dashed line is the same ZAMS, but shifted by $E_{B-V} = 0.55$. The arrow indicates the reddening law.

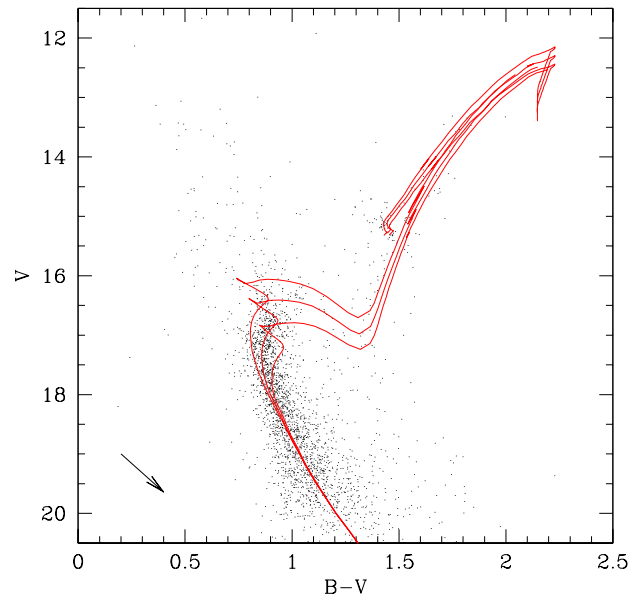


Figure 8. NGC 2158 data the V vs. $B-V$ diagram (points), as compared to Girardi et al. (2000a) isochrones of ages 1.58×10^9 , 2.00×10^9 , and 2.51×10^9 yr (solid lines), for the metallicity $Z = 0.0048$. A distance modulus of $(m-M)_0 = 12.8$, and a colour excess of $E_{B-V} = 0.60$, have been adopted. The direction of the reddening vector is indicated by the arrow at the bottom left.

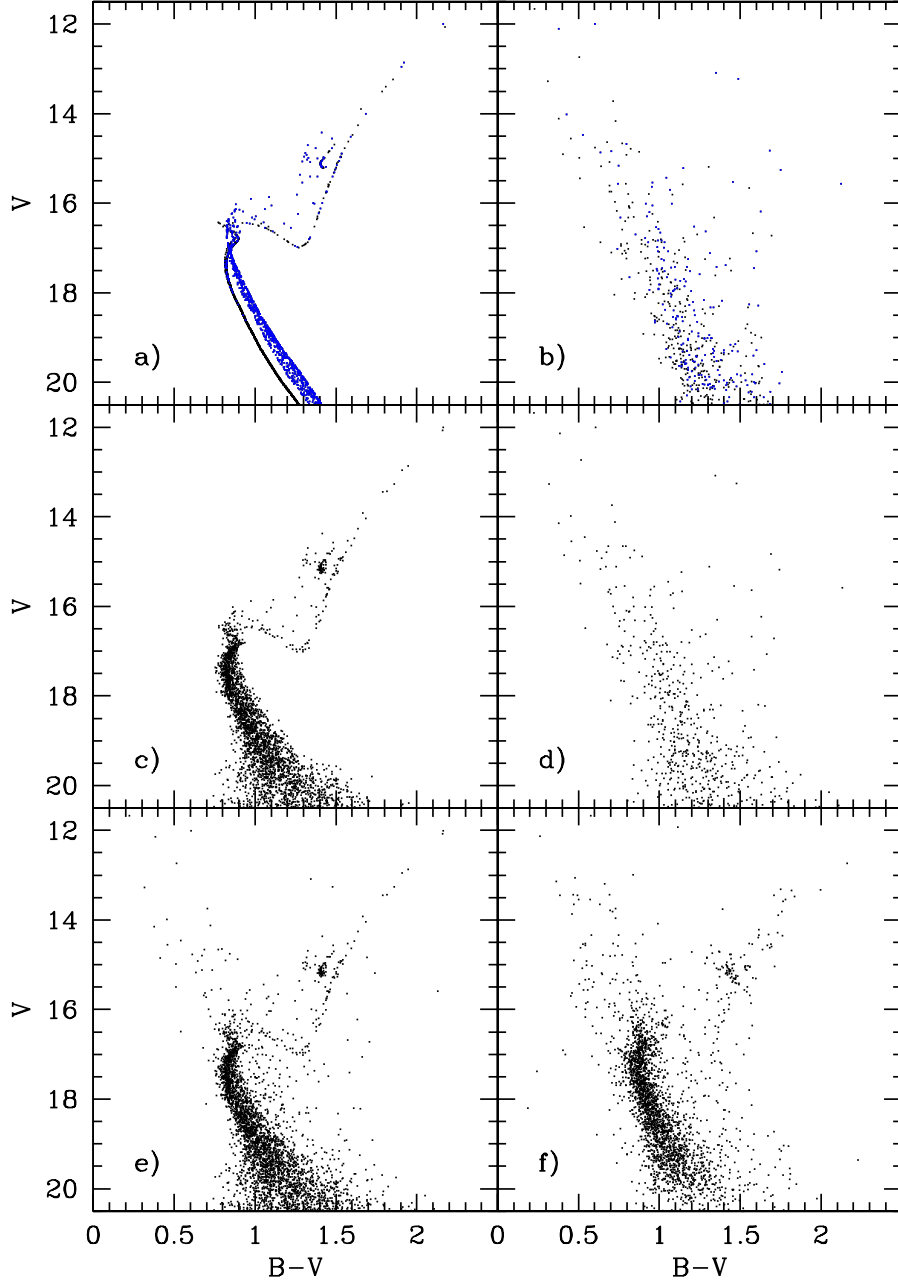


Figure 9. Simulations of NGC 2158 and its field in the V vs. $B - V$ diagram. **(a)** Simulation of a 2-Gyr old cluster with $Z = 0.0048$ and a initial mass of $1.5 \times 10^4 M_{\odot}$, based on the same isochrones, distance modulus and colour excess as in Fig. 8. We have assumed that 30 percent of the stars are binaries with mass ratios between 0.7 and 1.0. **(b)** Simulation of a $9 \times 11 \text{ arcmin}^2$ field centered at galactic coordinates $\ell = 186^{\circ}.64$, $b = +1^{\circ}.80$, performed with Girardi et al. (2001) Galactic model. Panels **(c)** and **(d)** are the same as **(a)** and **(b)**, respectively, after simulation of photometric errors. Panel **(e)** shows the sum of **(c)** and **(d)**, that can be compared to the observational data shown in panel **(f)**.

tic components – thin and thick disk, halo, and an extinction layer – adopting geometric parameters as calibrated by Groenewegen et al. (2001). The most relevant component in this case is the thin disk, which is modelled by exponential density distributions in both vertical and radial directions. The radial scale height is kept fixed (2.8 kpc), whereas the vertical scale height h_z increases with the stellar age t as

$$h_z = z_0(1 + t/t_0)^{\alpha} \quad (4)$$

with $z_0 = 95 \text{ pc}$, $t_0 = 4.4 \text{ Gyr}$, $\alpha = 1.66$. The simulated field has the same area ($9 \times 11 \text{ arcmin}^2$) and galactic coordinates ($\ell = 186^{\circ}.64$, $b = +1^{\circ}.80$) as the observed one for NGC 2158. The results are shown in Fig. 9(b). It is noteworthy that, in this direction, most of the Galactic field stars appear in a sort of diagonal sequence in the CMD, that roughly corresponds to the position of NGC 2158 main sequence.

- We then simulate the photometric errors as a function

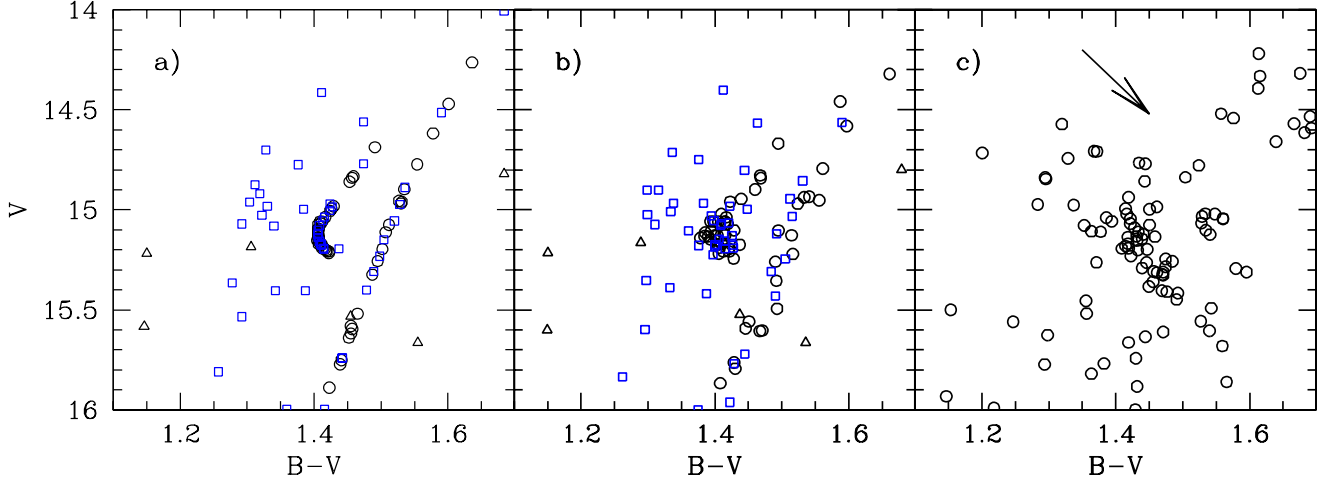


Figure 10. The same simulations of Fig. 9, but detailing the region of clump giants. (a) The simulated data. Circles are single stars in the cluster, squares are the binaries, and the few triangles are field stars. (b) The same as in panel (a), but including the simulation of photometric errors. (c) The observed data for NGC 2158. The arrow shows the reddening vector corresponding to $\Delta E_{B-V} = 0.1$.

of V magnitude, with typical values derived from our observations (see Fig. 3). The results are shown separately for cluster and field stars in panels (c) and (d) of Fig. 9.

- The sum of field and cluster simulations is shown in Fig. 9(e). This can be compared directly to the observed data shown in Fig. 9(f).

The comparison of these two latter panels indicates that the selected cluster parameters – age, metallicity, mass, distance, reddening, and binary fraction – really lead to an excellent description of the observed CMD, when coupled with the simulated Galactic field. The most noteworthy aspects in this comparison are the location and shape of the turn-off and subgiant branch, that are the features most sensitive to the cluster age.

Of course, there are minor discrepancies between the observed and simulated data, namely: (i) The simulated cluster is better delineated in the CMD than the data. This may be ascribed to a possible underestimate of the photometric errors in our simulations, and to the possible presence of differential reddening across the cluster (see next section). (ii) There is a deficit of simulated field stars, that can be noticed more clearly for $V < 16$ and $(B - V) < 1$. This is caused by the simplified way in which the thin disk is included in the Galactic model: it is represented by means of simple exponentially-decreasing stellar densities in both radial and vertical directions, and does not include features such as spiral arms, intervening clusters, etc., that are necessary to correctly describe fields at low galactic latitudes. Anyway, the foreground/background simulation we present is only meant to give us an idea of the expected location of field stars in the CMD.

Although these shortcomings in our simulations might probably be eliminated with the use of slightly different prescriptions, they do not affect our main results, that regard the choice of cluster parameters.

Then, we conclude that $(m - M)_0 = 12.8$ mag (3630 pc), $E_{B-V} = 0.60$, 2 Gyr, $Z = 0.0048$ ($[\text{Fe}/\text{H}] = -0.60$), and

$1.5 \times 10^4 M_\odot$, well represent the cluster parameters. All these values are uncertain to some extent:

- From Fig. 8, we can estimate a maximum error of 15 percent (0.3 Gyr) in the age. One should keep in mind, however, that the absolute age value we derived, of 2 Gyr, depends on the choice of evolutionary models, and specially on the prescription for the extent of convective cores. For the stellar masses involved ($M_{\text{TO}} \sim 1.5 M_\odot$ for NGC 2158), our models (Girardi et al. 2000a) include a moderate amount of core overshooting.
- Our best fit model corresponds to $E_{B-V} = 0.60$, which is compatible with the range $E_{B-V} = 0.55 \pm 0.1$ indicated in Sect. 5.1. The uncertainty of 0.1 mag in E_{B-V} causes an uncertainty of ~ 0.3 mag in the distance modulus (15 percent in distance).
- The metallicity cannot be better constrained from the CMD data, unless we have more accurate estimates of the reddening.
- The initial mass estimate depends heavily on the choice of IMF, that determines the mass fraction locked into low-mass (unobserved) objects. The value of $1.5 \times 10^4 M_\odot$ was obtained with a Kroupa (2001) IMF, corrected in the lowest mass interval according to Chabrier (2001; details are given in Groenewegen et al. 2001), and should be considered just as a first guess. At present ages, supernovae explosions and stellar mass loss would have reduced this mass by about 20 percent.

5.3 Red clump structure and differential reddening

Our cluster simulations also allows us to examine in better detail the observed structure of the red clump in NGC 2158. Figure 10 details the clump region in the CMD, for both simulations (panels a and b) and data (panel c). As can be readily noticed in panel (c), the observed clump appears as a diagonal structure, whose slope is roughly coincident with the reddening vector. In cluster simulations, however,

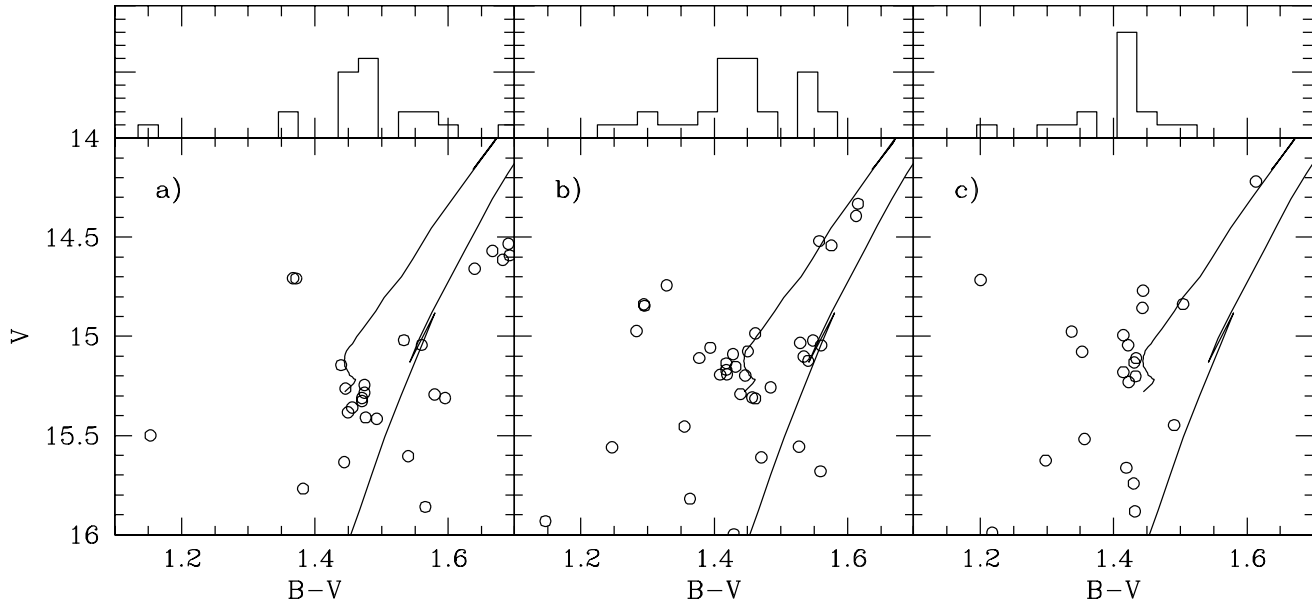


Figure 11. Bottom panels: The same as in Fig. 10, but now illustrating the stellar data at different intervals of galactic latitude, namely (a) $1^{\circ}.73 < b < 1^{\circ}.77$ (toward NE in Fig. 1), (b) $1^{\circ}.77 < b < 1^{\circ}.81$ (central part of the cluster), and (c) $1^{\circ}.81 < b < 1^{\circ}.85$ (toward SW). In all cases, only stars located at $186^{\circ}.58 < \ell < 186^{\circ}.69$ (a strip about $7'$ wide) were plotted. As a reference to the eye, we plot also the same 2-Gyr old isochrone as shown in previous Fig. 8. The panels at the top illustrate, for each case, the colour histogram of stars with $14.7 < V < 15.7$. Notice the progressive shift of the clump to the blue as b increases.

the clump is normally seen as a more compact structure. This can be appreciated in the simulations for single stars shown in Girardi et al. (2000b), where the model clumps are found to be more elongated in the top-bottom direction in the CMD, and not diagonally. The same result is found in Figure 10a, if we look only at the locus of single stars.

However, part of the clump widening might be caused by the presence of binaries, as shown by the different symbols in our simulations of panels (a) and (b). It turns out that binaries composed of clump plus turn-off stars are located at a bluer colour, and are slightly brighter, if compared to the locus of single clump stars. Thus, binaries tend to widen the clump structure along a direction that roughly coincides with the reddening vector. But anyway, as can be readily noticed from Fig. 10, binaries cannot account entirely for the clump elongation observed in NGC 2158.

Instead, since NGC 2158 is located very low in the Galactic plane, the observed clump morphology might well be caused by the presence of differential reddening over the cluster. We can get an estimate of the expected differential reddening, starting from simple models of the dust distribution in the thin disk. To this aim, we use the Girardi et al. (2001) Galactic model, assume a local extinction value of 0.75 mag/kpc in V (Lyngå 1982), and a diffuse dust layer of exponentially-decreasing density with a scale height equal to 110 pc . With these parameters, in correspondence of the NGC 2158 location we obtain a differential reddening of $\Delta E_{B-V}/\Delta b = -0.021 \text{ mag/arcmin}$ perpendicularly to the Galactic plane. This estimate has the right order of magnitude to explain the width of the observed clump.

In order to investigate whether this kind of picture is realistic, in Fig. 11 we plot the CMDs for NGC 2158, separated in different strips of Galactic latitude b . The 2-Gyr old

isochrone, located at a fixed position in all panels, allows an easy visualization of how the clump gets bluer at increasing b .[¶] Assuming that this effect is caused by differential reddening perpendicularly to the Galactic plane, we get an estimate of $\Delta E_{B-V}/\Delta b \simeq -0.011 \text{ mag/arcmin}$.

We conclude that NGC 2158 presents some amount of differential reddening. Along the $\sim 6'$ diameter of the cluster, this effect amounts to about $\Delta E_{B-V} \sim 0.06 \text{ mag}$. Since our previous determinations of the cluster age, distance, and reddening were based on the mean location of the observed stars, the correction of the data for differential reddening would not imply any significant change in the derived parameters.

6 CLUSTER KINEMATICS

The availability of mean radial velocity and proper motion measurements allows us to discuss in some detail the kinematics of NGC 2158. Radial velocity has been measured for 8 stars by Scott et al. (1995) and for 20 stars by Minniti (1995). These measurements have a comparable accuracy between 10 and 15 km/s. A systematic shift of about 10 km/s is likely to exist, in the sense that the mean radial velocity from Minniti (1995) is lower than that derived by Scott et al. (1995). Although Minniti (1995) mean radial velocity is based on better statistics, we shall present results based upon both the determinations.

Absolute proper motions have been derived by

[¶] A similar effect was also noticed for NGC 2158 main sequence stars.

Kharchenko et al. (1997), and amount to $\mu_x = +0.66 \pm 2.03$, $\mu_y = -3.23 \pm 2.16$, where $\mu_x = \mu_\alpha \cdot \cos\delta$ and $\mu_y = \mu_\delta$.

Following in details Carraro & Chiosi (1994b) and Barbieri & Gratton (2001) we derived the velocity components of NGC 2158 in a Galactocentric reference frame U , V and W . The results are summarized in Table 3.

By adopting the Allen & Santillán (1991) rotationally symmetric Galaxy mass model, we integrated back in time NGC 2158 orbit for a duration comparable with NGC 2158 age (see previous Sect. 5.2), in order to obtain estimates of its eccentricity, epicyclic (ω -) and vertical (z -) amplitude. These parameters, together with age and metallicity, are fundamental to place the cluster in the right disk population.

The orbit integration has been performed using a modified version of the second-order Burlish-Stoer integrator originally developed by S.J. Aarseth (private communication). We provide orbits both for the Minniti (1995) and Scott et al. (1995) mean radial velocity estimates. They are shown in the upper and middle panels of Fig. 12. The parameters are basically consistent, as listed also in Table 4. For the sake of the discussion, in the lower panel we show a new orbit determination for the open cluster NGC 2420, which roughly shares the same age (1.8 Gyr) and metallicity ($[\text{Fe}/\text{H}] = -0.42$) of NGC 2158 (Friel & Janes 1993; Carraro et al 1998). The orbit of NGC 2420 was previously computed by Keenan & Innanen (1974) who suggest that this cluster might have been disturbed in his motion around the Galactic center by the influence of the Magellanic Clouds, an hypothesis which sounds reasonable - the cluster has high eccentricity, large apogalacticon and stays most of the time relatively high above the galactic plane- but which deserves a further detailed numerical investigation.

Christian et al. (1985) argue about the possibility that NGC 2158 and NGC 2420 might share common properties and origin, since they are coeval and have very low metal abundances for open clusters of this age. It is therefore interesting to compare their orbits, also because NGC 2158 is even metal poorer than NGC 2420. With an eccentricity $e = (R_a - R_p)/(R_a + R_p) = 0.20$ - where R_a and R_p are the apo- and peri-galacticon, respectively - the cluster reaches a maximum distance of about 12 kpc from the Galactic Center in the direction of the anti-center, where it is located right now and where it probably formed. It remains relatively low in the Galactic disk, in a region populated by young and intermediate-age Population I objects. The only difference with this population is the rather low metal content, less than half the solar value.

Apparently, we are facing two significantly different orbits. NGC 2158 has an orbit more similar to normal Population I objects, whereas NGC 2420 possesses an eccentricity much higher than the typical Population I objects. Moreover, NGC 2420 is more distant than NGC 2158. NGC 2420 and NGC 2158 are not the only two cases of low metallicity intermediate-age clusters in the anti-center direction. From Carraro et al. (1998) we have extracted 10 clusters with age between 1.5 and 3.5 Gyr and low metal content ($[\text{Fe}/\text{H}] < -0.50$). All these clusters presently lie in a Galactic sector between $\ell = 135^\circ$ and $\ell = 225^\circ$. They are: NGC 2158, NGC 2204, NGC 2420, NGC 2141, NGC 2243, Tombaugh 2, Berkeley 19, 20, 21, 31 and 32. The common properties of these clusters suggest the possibility that they

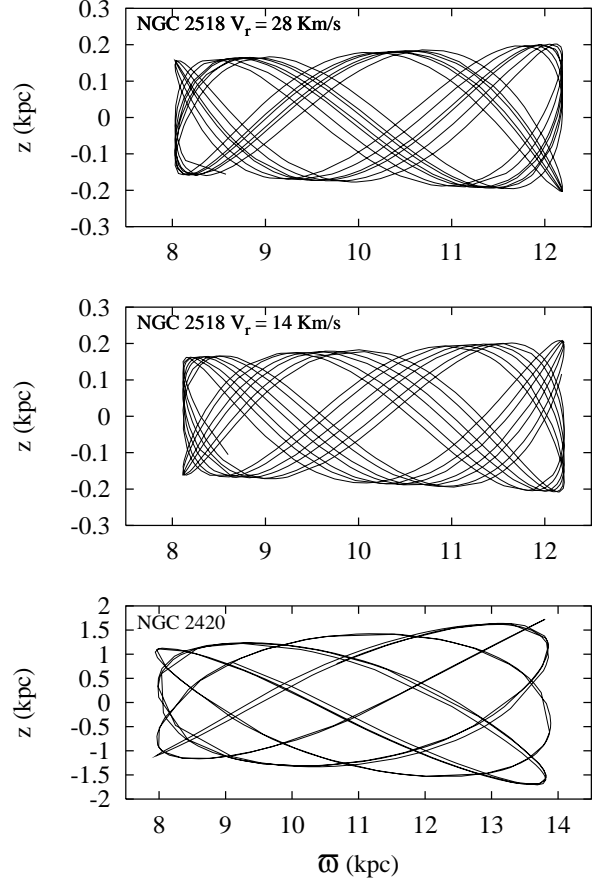


Figure 12. NGC 2158 orbit in the meridional plane. In the upper panel we display the orbit obtained by using the radial velocity estimate from Scott et al. (1995), whereas the middle panel shows the orbit obtained by adopting the radial velocity estimate from Minniti (1995). The lower panel presents the orbit of NGC 2420.

Table 4. NGC 2158 orbit's basic parameters.

	R_a kpc	R_p kpc	e	z_{\max} kpc
Minniti	12.21	8.11	0.20	0.21
Scott et al.	12.19	8.03	0.21	0.20

formed from the same material. Typically, the mean metal content of the Galactic disk at distances between 12 and 16 kpc ranges between $[\text{Fe}/\text{H}] = -0.50$ and $[\text{Fe}/\text{H}] = -0.70$, according to recent estimates of the Galactic disk metallicity gradient (Carraro et al 1998). Such a low metal content is compatible with the low density, hence low star formation, probably typical of that region. In this respect it would be interesting to compute Galactic orbits for all these clusters to check whether a trend exists to have more eccentric orbits at increasing Galactocentric distance in this region of the anti-center. This would help to better understand the structure and evolution of the outer Galactic disk.

Table 3. NGC 2158 basic kinematical parameters. The velocity components have been computed by adopting Minniti (1995, first row) Scott et al (1995, second row) radial velocity estimates.

$(m - M)_0$	X kpc	Y kpc	Z kpc	U km/s	V km/s	W km/s
12.80	12.11	-0.42	0.11	-7.99	-56.50	-16.88
				-21.88	-58.13	-16.45

7 CONCLUSIONS

We have presented a new CCD *UBVRI* photometric study of the intermediate age open cluster NGC 2158. From the analysis of the available data we can draw the following conclusions:

- The age of NGC 2158 is about 2 Gyr, with a 15 % uncertainty;
- the reddening E_{B-V} turns out to be 0.55 ± 0.10 and we find evidence of differential reddening (of about 0.06 mag) across the cluster;
- we place the cluster at about 3.6 kpc from the Sun toward the anti-center direction;
- combining together NGC 2158 age, metallicity and kinematics, we suggest that it is a genuine member of the old thin disk population.

ACKNOWLEDGEMENTS

We are very grateful to Chiara Miotto for carefully reading this manuscript, to Mauro Barbieri for NGC 2158 orbit integration, to Martin Groenewegen for the latest calibration of the Galactic model, and to Luciano Traverso, who secured the observations of January 7. We acknowledge also the referee, dr. G. Gilmore, for his useful suggestions. This study has been financed by the Italian Ministry of University, Scientific Research and Technology (MURST) and the Italian Space Agency (ASI), and made use of Simbad and WEBDA databases.

REFERENCES

- Allen C., Santillán A., 1991, *Rev. Mex. Astron. Astrof.* 22, 255
 Arp H., Cuffey J., 1962, *ApJ* 136, 51
 Barbieri M., Gratton R.G., 2001, *A&A* submitted
 Barmina R., Girardi L., Chiosi, *A&A* submitted
 Carraro G., Chiosi C., 1994a, *A&A* 287, 761
 Carraro G., Chiosi C., 1994b, *A&A* 288, 751
 Carraro G., Patat F., 1994, *A&A* 317, 403
 Carraro G., Ng Y.K., Portinari L., 1998, *MNRAS* 296, 1045
 Carraro G., Girardi L., Chiosi C., 1999, *MNRAS* 309, 430
 Carraro G., Hassan S.M., Ortolani S., Vallenari A., 2001, *A&A* 372, 879
 Chabrier G., 2001, *ApJ* 554, 1274
 Christian C.A., Heasley J.N., Janes K.A., 1985, *ApJ* 299, 683
 Elson R.A.W., Sigurdsson S., Davies M., Hurley J., Gilmore G., 1998, *MNRAS*, 300, 857
 Friel E.D., Janes K.A., 1993, *A&A* 267, 75
 Geisler D., 1987, *AJ* 94, 84
 Girardi L., Bressan A., Bertelli G., Chiosi C., 2000a, *A&AS* 141, 371
 Girardi L., Mermilliod J.-C., Carraro G., 2000b, *A&A* 354, 892

- Groenewegen M.A.T., Girardi L., Hadziminaoglou E., et al. 2001, *A&A*, submitted
 Lyngå G., 1982, *A&A* 109, 213
 Lyngå G., 1987, *The Open Star Clusters Catalogue*, 5th edition
 Keenan D.W., Innanen K.A., 1974, *ApJ* 189, 205
 Kharcenko N., Andruk V., Schilbach E., 1997, *Astron. Nach.* 318, 253
 Kroupa P., 2001, *MNRAS* 322, 231
 Minniti D., 1995, *A&AS* 113, 299
 Munari U., Carraro G., 1996a, *A&A* 314, 108
 Munari U., Carraro G., 1996b, *MNRAS* 283, 905
 Patat F., Carraro G., 1995, *A&AS* 114, 281
 Patat F., Carraro G., 2001, *MNRAS* 325, 1591
 Piersimoni A., Cassisi S., Brocato E., Straniero O., 1993, *Mem.S.A.It.* 64, 609
 Scott J.E., Friel E.D., Janes, K.A., 1995, *AJ* 109, 1706
 Schild R.E., 1983, *PASP* 95, 1021
 Schmidt-Kaler, Th., 1982, *Landolt-Börnstein, Numerical data and Functional Relationships in Science and Technology*, New Series, Group VI, Vol. 2(b), K. Schaifers and H.H. Voigt Eds., Springer Verlag, Berlin, p.14
 Trumpler R.J., 1930, *Lick Observ. Bull.* 14, 154
 Vallenari A., Carraro G., Richichi A., 2000, *A&A* 353, 147